Corrosion protection of bronze using 2,5-dimercapto-1,3,4-thiadiazole as organic inhibitor: spectroscopic and electrochemical investigations

Wafaa Qafsaoui, A. Et Taouil, M. W Kendig, O. Heintz, Hubert Cachet, Suzanne Joiret, Hisasi Takenouti

Corrosion protection of bronze using 2,5-dimercapto-1,3,4-thiadiazole as organic inhibitor: spectroscopic and electrochemical investigations

W. Qafsaoui[a], A. Et Taouil[b,*], M.W. Kendig[c], O. Heintz[d], H. Cachet[e], S. Joiret[e] and H. Takenouti[e]

[a] Laboratoire de l'Eau et de l'Environnement, Faculté des Sciences d'El Jadida, BP 20, 24000 El Jadida, Morocco. wqafsaoui@gmail.com

[b]Institut UTINAM, UMR 6213 CNRS, Université de Bourgogne Franche-Comté, 30 Avenue de l'Observatoire, 25009 Besançon Cedex, France. abdeslam.et_taouil@univ-fcomte.fr

[c]Kendig Research Associates LLC, 496 Hillsborough, Thousand Oaks, CA 91361. USA, martin.kendig@verizon.net

[d]Laboratoire ICB, UMR 6303 CNRS, Université de Bourgogne Franche-Comté, 9, Av. Alain Savary, 21078 Dijon Cedex, France. olivier.heintz@u-bourgogne.fr

[e]Sorbonne Universités, UPMC Univ Paris 06, CNRS, Laboratoire Interfaces et Systèmes Electrochimiques, 4 place Jussieu, F-75005, Paris, France.

hubert.cachet@upmc.fr; suzanne.joiret@upmc.fr; hisasi.takenouti@upmc.fr

Abstract

Effect of 2,5-dimercapto-1,3,4-thiadiazole (DMTD) concentration on the electrochemical behaviour of bronze was studied in 30 g L-1 sodium chloride (NaCl) by means of surface analyses and electrochemical techniques. Scanning Electron Microscopy (SEM) was used to observe surface morphology. Raman micro-spectroscopy was carried out to study chemical structure of deposited layers. X-ray photoelectron spectroscopy (XPS) enabled elemental characterization as well as molecular structure investigation. Finally, electrochemical polarization and impedance permitted a thorough study of corrosion protection behaviour reached through the presence of DMTD based organic layers on the surface. Above 1 mM, a fast adsorption of DMTD on copper (Cu) and lead (Pb) allows a thin and blocking film to be formed on bronze surface. DMTD prevents oxide formation at high concentrations and the surface film is mainly composed of Cu^{I}-DMTD and Cu^{II}-DMTD complexes as evidenced by spectroscopic techniques, with a bidentate adsorption at 1 mM and monodentate adsorption at 10 mM.

Keywords: Corrosion protection, Bronze, 2,5-dimercapto-1,3,4-thiadiazole, Electrochemical Impedance Spectroscopy, Raman spectroscopy, Neutral inhibition.

∗ Corresponding author: Tel: +33(0)381666863; E-mail: abdeslam.et_taouil@univ-fcomte.fr

1. Introduction

Copper and its alloys are among the first metals used by humans for technical and cultural/artistic purposes. Bronze or Cu-Sn alloys have ancient origins and appear in many cultural artefacts. In general, ancient bronzes have about 5% (wt) Sn content. The higher tin bronzes (11-12%) are particularly hard and thus was used industrially as bearing materials. High tensile strength also makes these materials the more structurally useful of Cu alloys. Their microstructure may be heterogeneous consisting of a dendritic structure with a Sn rich region which is highly unstable with respect to corrosion [1].

The rate of corrosion of bronzes in seawater or high chloride environments appears to increase with increasing composition of Sn as suggested by Thompson from a long term environmental exposure study of Cu alloys [2]. This was attributed to the high solubility of $SnCl_2$ in water. On the other hand, the corrosion rate for the Cu-Sn alloys in non-chloride media, mainly sulphate solutions, remains quite low and the trend in corrosion rate with Sn content is reversed with the higher Sn content leading to slower rates of corrosion [3].

Spontaneous formation of a protective layer or patina on bronze artefacts is considered to have aesthetic value. Many studies of the corrosion inhibition of these nominally 6% Sn patinated materials consider the interaction of the inhibitor with the oxidic patina [4-9]. Others have considered the more Sn rich alloys from a standpoint of the role of the alloy microstructure [10].

Corrosion rates from electrochemical and mass loss observation of historical artefacts are in good agreement [11]. This shows the validity of using electrochemical means to evaluate bronze corrosion.

Most of the corrosion inhibition of bronze has focused on the 6% Sn alloys which have been relevant to archaeological artefacts. The selected inhibitors for these materials were considered primarily from the inhibition of Cu by the benzotriazole (BTAH) inhibitor and analogs imidazoles [9-13]. A review of the inhibition of Cu and Cu alloys by BTAH found the inhibitor to perform well in non-polluted waters, but not so much in polluted waters containing sulfides [14]. A variety of thiadiazoles have been evaluated from the standpoint of being relatively environmentally innoxious [6]. In the same perspective, anti-bacterial drugs have been considered as viable inhibitors for bronze surfaces in mild acidic solutions [15]. Cano and Lafuente [9] provided a review of corrosion inhibitors for preservation of historical artefacts, and come to the conclusion that BTAH remains the best inhibitor. As mentioned previously, the higher Sn bronzes have industrial applications as a result of their relatively high hardness and mechanical strength. Walker [10] evaluated the performance of BTAH with the different microstructures of this alloy. He showed that during immersion of the alloy in aerated sea-water containing BTAH, inhibition occurred and that the reduced attack was preferentially on the Cu-rich phase. BTAH served as an anodic inhibitor for the Cu-rich phase.

Dithio compounds were shown to be particularly effective as corrosion inhibitors for Cu among which 1-pyrrolidinedithiocarbamate (PDTC) [16, 17] and 2,5-dimercapto-1,3,4-thiadiazole (DMTD) are important examples. In a very recent study dedicated to bronze corrosion inhibition by PDTC [18], we showed that this compound adsorbs on bronze surface, *via* interactions between sulphur atoms and Cu sites, to form Cu^{I}-PDTC complex. Besides, PDTC adsorption is so fast that it prevents oxides formation. The bronze surface is then protected by a thick, insulating and protective film. Regarding DMTD, Qin *et al* [19] showed corrosion

inhibition on Cu in acidic solutions by formation of self-assembled mono-layers. Yadav and Sharma [20] proved that the compound effectively inhibits Cu corrosion in 3.5% NaCl solution. Kendig and Hon [21] demonstrated that DMDT shows excellent oxygen reduction reaction (ORR) inhibition on Cu surfaces and can be encapsulated in a hydrotalcite matrix or a polyaniline matrix [22, 23]. DMTD was compared with Ce ions as an oxygen reduction reaction (ORR) inhibitor [24]. What makes DMDT somehow unique is that when oxidized, DMTD forms a disulfide polymer whom reduction releases the corrosion inhibiting monomer [25]. In light of these results, DMTD is a potential corrosion inhibitor for bronze, particularly in light of its ability to be stored and released when incorporated in thin films and coatings.

The objective of this study is to evaluate the effects of DMTD on corrosion inhibition of bronze in high chloride (30 g L^{-1} NaCl) environment. Specifically, this work aims at detailing interactions of DMTD with bronze surface that lead to corrosion inhibition. The study includes results from polarization curves, EIS measurements, SEM/EDS, Raman spectroscopy and XPS analyses. The overall objective is to understand the detailed molecular interactions of DMTD with bronze surface.

2. Experimental methods

2.1. Chemicals and materials

The studied alloy is an industrial bronze (used in aerospace and automotive industries) which composition is given in table 1 and was also used in our previous study [18]. This bronze is an alpha-cored bronze corresponding to the AFNOR norm "CuSn12". It consists of a dendritic structure rich in Cu in the centre and in Sn in the periphery. Non-miscible lead is observed in interdendritic spaces.

The disk electrodes of bronze along with those of pure Cu, Sn, Pb, Zn (Goodfellow, 99.999% of quality) were made of 5 mm diameter cylindrical rods. The rods were embedded into allylic

resin or a thermal shrinking sheath. Prior to this preparation, the lateral part of the cylinder rod was coated with a cataphoretic paint (PGG W975 + G323) to avoid the electrolyte infiltration. The electrode surface was then abraded under running water just before experiments, by rotating silicon carbide paper up to 1200 grade, and then rinsed thoroughly with deionized water.

Chemicals were purchased from Sigma Aldrich® (analytical grade). The blank corrosion test solution was prepared with NaCl, and DMTD ($C_2H_2N_2S_3$, M = 150.25 g mol^{-1}) was added as inhibitor.

2.2. Surface analyses

2.2.1. Scanning Electron Microscopy (SEM) / Energy Dispersive X-ray Spectroscopy (EDX)

A field emission gun scanning microscope (FEG-SEM, Zeiss, Ultra 55) coupled with energy-dispersive X-ray spectroscopy (EDX) was used to study surface morphology and composition. Element analyses were performed with a Quantax Bruker detector and data were analyzed by the Bruker Esprit software.

2.2.2. Raman micro-spectroscopy

Raman micro-spectroscopy analyses were carried out with a Labram-Jobin-Yvon spectrometer. The samples were irradiated with a He-Ne laser at $\lambda = 632.8$ nm at a power varied between 0.1 and 1 mW to avoid any thermal effect on the samples. A confocal microscope was used and the investigated area was limited to 5 μm^2 using an Olympus 80× Ultra Long Working Distance (ULWD) objective lens.

2.2.3 X-ray photoelectron spectroscopy (XPS)

XPS experiments were performed with Versaprobe PHI 5000 apparatus. Monochromated Al *Kα1* (1486.7 eV) was used for excitation with a circular spot of 200 µm of diameter and 50 W of power. The spectrometer was calibrated with adventitious carbon (C_{1s} at 284.7 ± 0.1 eV). The detection angle was 45°. The pressure in the UHV analysis chamber was less than 10^{-7} Pa.

2.3. Electrochemical measurements

Electrochemical measurements were carried out in aqueous solutions in a conventional three-electrode cell, using a Gamry potentiostat /galvanostat Model FAS-1 or 300C. The reference electrode was a saturated calomel electrode (SCE). The counter electrode was a platinum grid of a large surface area set close to the cell wall. The working disk electrode was faced towards the cell bottom under stationary conditions without any stirring. Corrosion test solution was 30 g L^{-1} NaCl, to which 10^{-4}, 10^{-3}, or 10^{-2} mol L^{-1} of 2,5-dimercapto-1,3,4-thiadiazole (DMTD) was added, as corrosion inhibitor. For each experiment, 100 mL of electrolyte was used. Corrosion tests were carried out under temperature control (20 °C) without purging dissolved oxygen.

2.3.1. Electrochemical polarization

Polarization measurements were performed after one hour immersion in the corrosion test solution (with or without DMTD). The curves were plotted from two independent measurements in a new test solution for each run: one from the open circuit potential towards about -1.5 V / SCE and another from the open circuit potential to about +1.5 V / SCE at a potential scan rate of 1 mV s^{-1}. Three replica experiments were carried out for each experimental condition.

2.3.2. Electrochemical impedance

The impedance measurements were performed applying 10 mV_{rms} from 100 kHz to 10 mHz taking 10 points per decade at different immersion times up to 24 hours. Experiments were carried out at open-circuit potential. The data were fitted by Simad software, a lab-made software using a simplex regression method.

3. Results and discussion

3.1. Surface analyses

3.1.1. SEM and EDX analyses

The bronze surface was examined by SEM after 24 h immersion in 30 g L^{-1} NaCl, without and with different DMTD concentrations (Fig. 1). In the blank test solution, the surface morphology (not shown) is quite similar to that observed in 0.1 mM DMTD (Fig. 1a) revealing a grainy microstructure, basically corresponding to the formation of an oxide film [18]. For higher DMTD concentrations i.e. 1 and 10 mM (Figs. 1b and c), the formation of oxides or corrosion products on the electrode surface was markedly delayed by the presence of a homogeneous organic-like film. This is shown by the EDX results displayed in table 2 and confirming the presence of sulphur within the films formed at these two DMTD concentrations, and only traces of oxides, likely indicating a fast adsorption of DMTD on bronze surface preventing the oxides film formation. Similar results were observed in the case of PDTC adsorption on bronze [18]. It is important to note that, despite their presence in DMTD, the carbon and nitrogen were not analyzed quantitatively. Besides, as for the blank, no trace of sulphur was detected at 0.1 mM DMTD due to very weak or no adsorption of DMTD. It can be concluded from these results that a layer, almost free from oxides, forms on bronze surface in presence of 1 mM and 10 mM DMTD.

3.1.2. Raman micro-spectroscopy analyses

Raman micro-spectroscopy spectra were recorded on the bronze surface after 24 hours exposure to 30 g L^{-1} NaCl solution, without or with addition of DMTD, in order to investigate the presumed interactions of DMTD with the surface mainly at 1 mM and 10 mM. Fig. 2-shows the spectra collected in addition to those of pure DMTD molecule in powder state and Cu^{II}-DMTD complex. Note that without or with 0.1 mM DMTD, Raman spectra are similar and show up Cu_2O layer formation indicated by the presence of a doublet around 500 and 600 cm^{-1} [26]. This result, in accordance with the SEM and EDX analyses, suggests that 0.1 mM is a concentration too low to enable the formation of a DMTD layer. However, at 10 mM the spectrum shows the absence of Cu_2O band and the presence of some bands of DMTD molecule, denoting potential interactions between DMTD and bronze to form a surface film. Moreover, the similarity between the complex spectrum and that obtained at 10 mM DMTD suggests that the film formed at this concentration is composed, at least, of a Cu^{II}-DMTD complex. If Cu_2O forms then its quantity must be extremely low to be detected. DMTD may also react with Cu^{+} ions. However, due to inability to form Cu^{I}-DMTD complex in solution no spectrum was collected for comparison.

In Fig. 3 are reported Raman spectra of bronze and copper electrodes recorded after 24 hours immersion in 30 g L^{-1} NaCl with 1 mM or 10 mM DMDT. This figure clearly shows that the spectra are similar for bronze and copper at the same concentration, maybe with a better resolution for copper electrode. However, they are clearly different when going from 1mM to 10mM. This concentration effect on DMDT adsorption on Ag was already reported [27] and studied from 10^{-2} to 5 mM. According to the authors, DMDT is present in two different configurations of adsorption with a slow transition when the molecule concentration goes from 10^{-2} to 5 mM. This is also the case here but as the concentration variation is rather low, Raman spectra are the sum of the two contributions which may correspond to two species A and B.

This can be visualized clearly from the main band at 1370-1420 cm^{-1} which is the convolution of two bands one at 1370 cm^{-1} predominant at 1mM and one at 1420 cm^{-1} predominant at 10 mM.

In order to shed more light on these results, Raman bands are reported in table 3 with A and B species presenting the more intense bands at 1 mM and at 10 mM DMTD respectively, together with DMDT molecule ones and from literature those corresponding to monoanion (monothiolate form: $DMTD^{-}$) [28], dianion (dithiolate form: $DMTD^{2-}$) [27, 28] and Raman bands assignments [27-30].

Literature survey on DMDT adsorption on Ag [27, 29], Au [29, 31] and Cu [31-33] provides a significant variety in adsorption configurations (S bound, N bound , standing up at low concentration and lying flat at high concentration, DMDT dimerization, polymeric complex Cu-DMDT) together with discussions on the thiol / thione tautomerism.

From this study the following conclusions can be drawn:

- the absence of S-H vibration in Raman spectra indicates an adsorption of thiolate anion on the metal surface,

- the absence of a sharp and intense band at 530 / 540 cm^{-1} (S-S stretching) precludes the formation of DMDT dimers,

- the close similarity of A spectrum with dithiolate one's implies a bidentate adsorption by the two S^{-} at low concentration (1 mM),

- at higher concentration (10 mM), B spectrum should be related to monothiolate one's essentially through the wavenumber position of C=N stretching 1410 cm^{-1} (1455 cm^{-1} for DMDT, 1405 cm^{-1} for $DMDT^{-}$ and 1375 cm^{-1} for $DMDT^{2-}$) and of C-S-C stretching 660 cm^{-1} (650 cm^{-1} for DMDT, 665 cm^{-1} for $DMDT^{-}$ and 670 cm^{-1} for $DMDT^{2-}$), adsorption taking place in monodentate form giving a less symmetric configuration and so a higher number of

Raman bands as observed. In this configuration, S-H vibration of unbonded thiol is expected but not observed in the experimental spectrum.

Fig. 4 shows a schematic representation of DMTD adsorption on bronze surface at 1 mM and 10 mM.

Transition from dianion to monoanion form, when increasing DMTD concentration from 1 to 10 mM, can also be viewed as a consequence of a better corrosion inhibition. Lower corrosion current is also associated to lower pH rise due to oxygen reduction promoting the acidic form of the thiolate / dithiolate couple.

3.1.3. XPS analysis

XPS measurements were performed on bronze surface after 24 hours immersion in 30 g L^{-1} NaCl solution without or with 10 mM DMTD. Survey spectra are presented in Fig. 5. It should be pointed out that, in contrast to Raman spectra, the obtained spectrum for 1 mM DMTD (not shown) is similar to that recorded for 10 mM.

For the layers formed on bronze, in the blank test solution and 0.1 mM DMTD, the spectrum shows peaks of Cu, Sn, Pb, C and O elements. The presence of the oxygen peak indicates that bronze surface is oxidized in chloride solutions, which is consistent with EDX and Raman results. O1s peak may also originate from oxidized atmospheric species or water molecules that remained on the surface after sample drying [34]. The carbon peak is ascribed to adventitious atmospheric species that can adsorb on bronze surface during sample preparation. Actually, when copper alloys are exposed to an open atmosphere during sample preparation before analysis, oxidation of metallic Cu is inescapable and atmospheric species can adsorb on the surface [34-36]. After immersion in the solution containing 10 mM DMTD, changes are visible on survey spectrum. Foremost, the nonappearance of Sn and Pb signals proves a substantial coverage of the bronze surface in the presence of DMTD, as previously observed in the case of PDTC [18]. Moreover, as evidenced by the appearance of N and S peaks, and the increased

intensity of C peak, the surface electrode is covered by a layer containing species from DMTD compound. In the same way, the peak intensity of oxygen is relatively small compared to that observed for the blank. DMTD adsorption on bronze surface is then presumably fast preventing or reducing the amount of oxide formed as suggested by the above results. This native oxide that forms unavoidably during sample preparation and the immersion procedure, may be buried beneath the DMTD layer. In fact, it is known that this oxide easily chemisorbs thiol compounds [37-39]. On the other hand, as the samples were immersed in chloride solutions, a peak representing Cl compounds could be expected. However, they are not present on the surface since Cl2p peak is missing around 200 eV. Thus, Cl species are not involved in the blank nor in DMTD modified surface layers. The same was previously obtained for PDTC treated copper [40] and bronze [18]. Similar results were observed on Cu with different other organic molecules [34-36, 38].

Fig. 6 shows Cu2p and CuLMM peaks obtained from the layers formed without and with 10 mM DMTD. In general, Cu2p spectrum of Cu is composed of $Cu2p_{3/2}$ peak at 932.20-933.10 eV and $Cu2p_{1/2}$ at 952.45-952.56 eV [36,41]. This spectrum indicates the presence of Cu^{II} species when typical shake-up satellites are located around 942.5 eV, approximately 10 eV above the main $Cu2p_{3/2}$ peak [41,42] (dashed lines in Fig. 6). However, for copper metal (Cu^0), Cu_2O and other Cu^I species, $Cu2p_{3/2}$ peak is located at almost the same binding energy (within ± 0.1 eV) [42]. In contrast, Auger CuLMM spectra of Cu and Cu^I compounds are significantly different and can be differentiated, since metallic Cu^0 shows a CuLMM peak at a kinetic energy of 919 eV and that of Cu_2O and Cu^I species appears 2 eV lower, around 916.7 eV [41-43].

For both films formed in the blank and 10 mM DMTD, the peaks located around 932.5 eV and 916.3 eV in $Cu2p_{3/2}$ and CuLMM range, respectively, prove that copper is mainly under Cu^I form [18,42-44]. Cu_2O forms thereby on bronze surface, in the blank test solution, in agreement with EDX and Raman results. As for the film formed in DMTD, Cu^I-DMTD complex may form

above a thin layer of Cu_2O [18,45]. Moreover, the slight shift to higher energies for Cu2p doublet peak after DMTD modification supports this assumption and suggests the presence of bonds between Cu^I and S atoms of DMTD [46,47] which indicates Cu^I-DMTD formation. Furthermore, Cu2p spectrum shows a shoulder around 934.3 eV and characteristic shake-up satellites on the higher binding energy side of the doublet suggesting the presence of Cu^{II} species [41,42], namely Cu^{II}-DMTD as suggested by Raman results.

To sum up, surface analyses showed that Cu_2O layer forms on bronze surface in 30 g L^{-1} NaCl and that no insulating film forms in the presence of 0.1 mM DMTD. However, at 1 mM and 10 mM, DMTD seems to readily adsorb on a weakly oxidized bronze surface. The film formed is composed of Cu^I-DMTD and Cu^{II}-DMTD complexes. Furthermore, DMTD adsorption is bidentate at 1 mM and monodentate at 10 mM.

3.2. Electrochemical measurements

3.2.1. Potentiodynamic polarization

3.2.1.a. Effects of DMTD concentration on bronze behaviour in 30 g L^{-1} *NaCl*

Fig. 7a compares the corrosion potential (E_{corr}) change as a function of immersion time of bronze electrode without or with different DMTD concentrations in 30 g L^{-1} NaCl. For the blank test solution, E_{corr} goes from -212 to -217 mV, in 30 seconds, then remains almost constant during the entire immersion period. Cu_2O formation on bronze, as suggested by Raman and XPS results, is fast in chloride media.

In the presence of 0.1 mM DMTD, E_{corr} tends towards more cathodic values (by about 35 mV) during 70 seconds, then increases continuously to a near constant value of -242 mV, which is 25 mV more cathodic than that measured in the blank solution. According to surface analyses, the film formed at this concentration is similar to that obtained without DMTD and consists of

Cu_2O. However, E_{corr} variation during immersion exhibits a different behaviour of the interface during the first seconds of immersion, denoting probable interactions between DMTD and the bronze surface in competition with Cu_2O formation. Corrosion products of DMTD at 0.1 mM are likely non-adherent or their quantity is too low to be detected.

Addition of 1 mM DMTD leads to a significant decrease of E_{corr} values during the first seconds of immersion (~ 20 s) followed by a gradual increase to about -300 mV. This result suggests that DMTD adsorbs readily on the bronze surface lowering E_{corr} to more cathodic values by decreasing the partial cathodic current density. DMTD may adsorb on the cathodic sites first, at the immersion. Afterwards, the increase in E_{corr} values may be due to DMTD desorption from the cathodic sites or its adsorption on the anodic ones. Nevertheless, it is unlikely that DMTD desorbs since surface analyses assert the formation of a DMTD layer. The same behaviour was observed, in a previous study, on copper in presence of PDTC [40]. The results obtained, by means of EIS measurements, showed that the charge transfer resistance R_t increases continuously during the decreasing and increasing steps of E_{corr} at the first immersion, denoting that PDTC adsorbs first on the cathodic sites then on the anodic ones to form a protective layer. According to surface analyses results and E_{corr} evolution during immersion, the same conclusion may be drawn for DMTD adsorption on bronze.

As far as 10 mM concentration is concerned, a fast increase of E_{corr} values, towards anodic potentials, may be observed during the first seconds of immersion then an almost constant value of -310 mV is reached after about 3 minutes. In agreement with the above results, it could be assumed that at 10 mM, DMTD adsorption is too fast to be observed from the beginning and only its adsorption on the anodic sites is clearly displayed in such curves.

The results of potentiodynamic measurements are given in Fig. 7b for bronze in 30 g L^{-1} NaCl in the absence and presence of DMTD. Anodic and cathodic characteristics were

measured by independent cathodic and anodic scan experiments as stated in the experimental section.

In the absence or presence of 0.1 mM DMTD, polarization curves are similar and display high current densities. E_{corr} values are close since the one measured at 0.1 mM is barely 25 mV more cathodic than that recorded in the blank. The anodic branch is typical of copper [48-51] and bronze [18] electrodes in highly concentrated chloride media: from lower over-potentials to a peak current density located around 0.083 V, copper dissolves. The following region of decreasing currents is due to CuCl formation and finally a slight increase in current density leading to a limiting value results from $CuCl_2^-$ formation. As for the cathodic branch, a peak around -1 V superimposed to the diffusion-limited current of oxygen reduction (ORR) is due to the reduction of tin species [52] and Cu_2O [16,40,53]. The quantity of these Sn and Cu corrosion products, formed in 0.1 mM DMTD, is very likely smaller since the current density of the corresponding reduction peak is lower. On the other hand, one can notice the absence of a cathodic peak corresponding to the reduction of corrosion products formed with DMTD during immersion. It could be then assumed that DMTD species do not adhere to the bronze surface and consequently are not part of the surface layer which is in accordance with surface analyses. Moreover, the minor quantity of Cu and Sn oxides formed during immersion may suggest a detrimental effect of DMTD at 0.1 mM.

In contrast, the peak observed around -560 mV for both films formed in 1 mM and 10 mM DMTD containing solutions, could be clearly ascribed to the reduction of DMTD complexes formed during immersion [18]. This peak that appears at a relatively important cathodic overvoltage suggests that these products are bonded to the electrode surface as suggested by surface analyses. In addition, polarization curves recorded at these higher DMTD concentrations are similar since the corresponding E_{corr} values are closer as well as the anodic and cathodic current densities that are considerably lowered. However, differences are observed

on the anodic branches of these curves that provide additional information regarding the anodic behavior of films formed at 1 and 10 mM. Actually, anodic plateaus are obtained for the films formed at both concentrations. Nevertheless, the one formed at 1 mM DMTD seems to be protective on a limited potential domain and weakened above 0.5 V since an increase in the current density starts at this potential. In contrast, a large anodic plateau of at least 1.8 V is obtained in the case of the film formed at 10 mM. It could be then concluded that a substantial inhibitive effect is obtained when the film is formed in presence of 10 mM DMTD. This is assuredly the result of DMTD adsorption on bronze surface, in monodentate form, as predicted by Raman analyses.

DMTD is a diacid with pKa values of -1.36 and 7.5 [54,55]. As our solution pH is about 6.5, it is mainly present in the monosalt form. Electrochemical behavior of this monoacid has been extensively studied in the literature [56,57]. Its oxidation forms a dimer through disulfide bridges (-S-S-) which oxidation leads to a one-dimensional polymer chain. These reactions are reversible and the reduction of the polymer leads to the dimer which reduction leads to the monoacid monomer. All these reactions occur through formation and breaking of sulfur-sulfur bonds. However, in 1 mM DMTD solution Raman results showed bidentate adsorption through exocyclic sulfur atoms which therefore cannot react to form dimers or polymers. In 10 mM DMTD solution, Raman experiments revealed monodentate adsorption. In this case, dimer formation would have theoretically been possible through coupling of thiol groups to form disulfide bridges. However and above all, no signal of DTMD oxidation is observed during electrochemical polarization on bronze (for 1 and 10 mM DMTD solution) which precludes the formation of dimers or polymers on bronze surface. Indeed, electrochemical oxidation of

DTMD and formation of dimers or polymers would have led to noticeable oxidation peaks as shown in previous studies [56, 57].

3.2.1.b. Comparison of 10 mM DMTD effects on bronze and pure metals (Cu, Sn, Zn, Pb) in 30 g L^{-1}*NaCl*

Effects of 10 mM DMTD on pure metals were investigated in 30 g L^{-1}, by means of polarization curves plots, in order to assess the potential interactions between DMTD and metal alloying elements in bronze. The curves obtained for Sn, Zn, Cu and Pb electrodes, without and with 10 mM DMTD, are displayed in Fig. 8. It is obvious that DMTD has a damaging impact on Sn and Zn electrodes, since the cathodic and anodic current densities are drastically increased compared to those obtained in the blank test solution. In contrast, the effect of DMTD is beneficial on Cu and Pb electrodes as the current densities are significantly lowered, revealing a significant mixed inhibitive effect in this chloride medium. Similar results were observed previously with PDTC [18]. It can be then concluded that the good corrosion protection obtained in the presence of 1mM and 10 mM DMTD is due to preferential interactions of DMTD with Cu and Pb contained in the alloy. It is obvious that, because of the low Pb content, only the Cu responses are evidenced by the surface analyses.

3.2.2. EIS measurements

3.2.2.a. Effects of DMTD concentration on EIS plots

EIS measurements were performed in 30 g L^{-1} NaCl to characterize the bronze electrode behaviour as a function of DMTD concentration and immersion times. All measurements were performed at E_{corr} to assess the interfacial behaviour under usual conditions of use and to estimate the electrical properties of the surface film as formed at various immersion periods.

The obtained Nyquist diagrams after 24 hours immersion in 30 g L^{-1} NaCl, without and with different concentrations of DMTD, are displayed in Fig. 9. It can be clearly seen that DMTD has an appreciable effect on bronze behaviour at 1 and 10 mM. In contrast, the insert exhibits a

detrimental effect of DMTD at 0.1 mM since the magnitude of the EIS spectrum recorded at this low concentration is reduced compared to that obtained in the blank test solution. This is consistent with the above results that ascribed a pernicious effect of DMTD on Sn and Zn corrosion leading to reinforced corrosion processes, mainly observed at this low DMTD concentration. The same shape of diagrams is observed throughout the immersion period for all studied DMTD concentrations. These spectra are in fact a convolution of three capacitive loops although not well resolved. As previously stated for bronze covered by patinas [6, 7], and in the case of the PDTC effect on bronze [18] and copper [16], the electrode response can be described by the electrical equivalent circuit depicted in Fig. 10. This circuit is based on the combination of three resistance-capacitance parallel elementary circuits, each one having a well-defined physical meaning: the high frequency (above 10 Hz) contribution (R_f, C_f) is ascribed to the dielectric character of the corrosion products (C_f) due to the formation of a surface layer that may be influenced by DMTD addition and by the ionic conduction through the pores of the film (R_f). The medium frequency (0.1-1 Hz) contribution (R_t, C_d) represents the double layer response of the bronze / electrolyte interface accessible through the surface film porosity (C_d) coupled with the charge transfer resistance (R_t). The low frequency (below 0.1 Hz) part (R_F, C_F) represents the contribution of possible additional faradaic processes at the metal surface as copper oxidation-reduction for instance. R_F is attributed to the rate of the process and C_F the corresponding pseudo-capacitance.

In the present impedance model, instead of using a constant phase element (CPE), the non-ideal character of each resistance-capacitance (R, C) contribution is represented by an expression identical to the symmetric frequency dispersion of dielectrics. It means that the impedance Z of any (R, C) loop is written as:

$$Z(\omega) = \frac{R}{1+(j\omega RC)^n} \quad (1)$$

The quantities n_f, n_d and n_F are Cole-Cole coefficients (in between 0 and 1) accounting for the depressed feature of the capacitive loops pointed out in Nyquist diagrams [58, 59]. $Z(\omega)$ extends significantly over about two decades of frequency with respect to the characteristic frequency $(2\pi RC)^{-1}$ as long as the Cole-Cole coefficient "n" is close to unity. As for CPE, the real part of the equivalent complex capacitance $C^*(\omega) = (j\omega Z)^{-1}$ is frequency dependent and it must be kept in mind that C represents the value of the capacitance at the frequency $(2\pi RC)^{-1}$, at the maximum of the capacitive loop in the Nyquist representation.

The most relevant results provided by EIS experiments about the inhibitive effect of DMTD are illustrated in Fig. 11. These figures display the variations of the fitted parameters (R_f, C_f) and (R_t, C_d) as a function of DMTD concentration and immersion time. As expected according to the above results, similar behaviour of the interface is observed in both the blank and 0.1 mM DMTD containing solutions. The film resistance R_f (Fig. 11a) is of the order of a few Ω cm^2 and the transfer resistance R_t (Fig. 11c) around 10^3 Ω cm^2. The film capacitance C_f (Fig. 11b) is dominated by corrosion products, reaching about 3 μF cm^{-2} for the blank and 20 μF cm^{-2} for 0.1 mM DMTD suggesting that film formed at this low concentration is thinner which is in accordance with polarization results. As for the interfacial capacitance C_d (Fig. 11d), the values range between 70 and 100 μF cm^{-2} for both the blank and 0.1 mM. On the other hand, a drastic change is observed as soon as the DMTD concentration is equal or above 1 mM. The formation of a blocking film is clearly evidenced by the increase of R_f up to 10^5 Ω cm^2 and that of R_t up to 3 10^5 Ω cm^2. Inversely, a decrease of C_f by an order of magnitude is the signature of a relatively thick film due to DMTD deposition. The blocking character of this surface film, as reducing the active metal surface, is well verified by the sharp decrease of the interfacial capacitance C_d of about two orders of magnitude compared to the blank and 0.1 mM DMTD.

For the low frequency region, the (R_F, C_F, n_F) fitted parameters were evaluated with an important extrapolation. Furthermore, the Cole-Cole coefficient n_F was found far from unity. As a consequence, the only relevant information concerns the amplitude of this low frequency contribution as measured by R_F. Fig. 12a shows the change of R_F with immersion time and DMTD concentration. Low values are observed for the blank and 0.1 mM DMTD corroborating the fact that no protective effect occurs at this low DMTD concentration. The blocking character of the interface observed at DMTD concentrations higher or equal to 1 mM is expressed by an increase of about two orders of magnitude of R_F with a trend similar to that observed for the resistance R_t.

It is worthwhile to mention that EIS spectra obtained with DMTD do not show a marked diffusional behaviour as previously observed with PDTC (Fig. 6 in [18]). It can be then stated that the protective layer formed with DMTD is thinner than the one formed with PDTC on bronze in chloride media.

3.2.2.b. Polarization resistance R_p

The polarization resistance R_p, that is better correlated with corrosion rate [7, 60], is given by the sum of the resistances R_t and R_F since the film resistance R_f is a non-faradic quantity:

$$R_P = R_t + R_F \quad (2)$$

Fig. 12b displays the variation of R_p as a function of time in 30 g L^{-1} NaCl without and with different concentrations of DMTD. A transition from active to passive systems is clearly highlighted when going from the blank and 0.1 mM DMTD to 1 and 10 mM DMTD. Indeed, along the whole immersion period, R_p values are low and moving closer to 17 kΩ cm^2 and 7 kΩ cm^2 in the blank and the solution containing 0.1 mM DMTD, respectively. This emphasises the noxious effect of DMTD on bronze at this low concentration. In contrast, significant values

of the polarization resistance R_p, approaching 1 MΩ cm², are obtained for 1 and 10 mM. The inhibitive effect of DMTD is, as expected, important at these higher concentrations and approximates 99%.

3.2.2.c. Film thickness δ

The thickness δ of the layers formed on bronze surface at E_{corr}, in 30 g L^{-1} NaCl without or with DMTD, may be estimated from both the film capacitance C_f deduced from the fitting of EIS data, or C_∞ the capacitance defined as the high frequency limit of the real part of the complex capacitance [18,61] using the following equation:

$$\delta = \frac{\varepsilon \varepsilon_0}{C} \quad (3)$$

C being the film capacitance (C_f or C_∞), ε_0 the vacuum permittivity and ε the film permittivity that was assumed approximating 10 for oxides film formed in the blank and 0.1 mM DMTD, and closer to 4 for those formed in 1 and 10 mM DMTD containing solutions.

Fig. 13 shows the variation of the surface film thickness, obtained from both C_f and C_∞, with immersion time and DMTD concentration. First of all, it can be seen that δ values calculated from C_∞ are slightly higher than those obtained from C_f. This is due to the fact that when the film thickness is calculated from C_∞, the estimated value is the highest thickness of the film since C_∞ is graphically determined as the high frequency limit and is independent of any interface modelling. In contrast, the fitting of EIS data take into consideration the dispersion of the capacitance values with frequency and C_f is a central value in the distribution. C_f value is therefore slightly higher than C_∞ one and consequently the thickness estimated from C_f is slightly lower. In the present study, dealing with bronze / NaCl + DMTD interface, both thickness estimations lead to closer values of δ since the Cole-Cole coefficient n_f is close to 1 due to a weak frequency dispersion of the film capacitance C_f.

Regarding the change in film thicknesses depending on the concentration of DMTD, a plateau at about 6 nm is obtained after a few hours of immersion. In the presence of 1 mM, the film is regularly and continuously growing, even after 24 hours. For comparison the thickness of films formed with DMTD is about one order of magnitude lower than those formed with PDTC [18].

4. Conclusion

In chloride environments, native Cu_2O oxide forms on bronze surface as a protective layer. This protection may be improved by addition of organic compounds that are known to have a good interaction with copper, since it is a major constituent of the alloy. In this way, the present study was devoted to the effect of 2,5-dimercapto-1,3,4-thiadiazole (DMTD) on bronze surface in 30 g L^{-1} NaCl. Electrochemical and long-term immersion tests (polarization curves and electrochemical impedance spectroscopy), coupled with surface analysis (SEM/EDX, XPS, Raman spectroscopy) investigations have been performed.

The main obtained results are summarized in the following points:

- Cu_2O is the main constituent of the layer formed on bronze surface in NaCl solution without or with 0.1 mM of DMTD. However, the oxide layer formation is hampered since the charge of the corresponding reduction peak is lower than that obtained in DMTD free solution.
- At higher concentrations, DMTD readily adsorbs on a weakly oxidized bronze surface and thus hinders the oxide evolution leading to the formation of a mainly organic surface layer.
- This fast adsorption, that is bidentate at 1 mM and monodentate at 10 mM, results in the formation of a few nanometers thick layer and occurs on Cu-rich regions via S atoms of DMTD. Moreover, DMTD has a good interaction with Pb since it decreases the kinetics of the anodic and cathodic processes in chloride media, for a pure Pb electrode. However, this interaction could not be highlighted in this study because of the small amount of Pb contained in the bronze.

- Surface analyses showed that the surface film is composed essentially of Cu^{I}-DMTD and Cu^{II}-DMTD complexes.
- At 1 mM DMTD and above, the polarization resistance is as high as 1 MΩ cm^2 for a film thickness lower than 10 nanometers.
- The film formed during immersion at 10 mM DMTD is stable and resistant even at high anodic overvoltage, since a current density plateau is obtained over a large potential domain, demonstrating that DMTD film is highly blocking and DMTD is a very efficient corrosion inhibitor of bronze in chloride media.

Acknowledgements

The University of El Jadida who authorized Pr. W. Qafsaoui to attend the LISE before the end of University year is gratefully acknowledged.

The authors thank F. Pillier for SEM analyses.

References

[1] Shreir LL, Jarman RA, Burstein GT (1994) Copper and Copper Alloys. In: Corrosion, Metal / Environment Reactions, vol 1. Butterworth-Heinmann, London, pp 38-75

[2] Thompson DH (1968) Atmospheric Corrosion of Copper Alloys. In: Metal Corrosion in the Atmosphere, ASTM STP 435. American Society of Testing and Materials, pp 129-140

[3] Muller J, Laïk B, Guillot I (2013) α-CuSn bronzes in sulphate medium: Influence of the tin content on corrosion processes. Corros Sci 77:46-51

[4] De Oliveira FJR, Lago DCB, Senna LF, De Miranda LRM, D'Elia E (2009) Study of patina formation on bronze specimens. Mater Chem Phys 115:761-770

[5] Otmačić Ćurković H, Kosec T, Marušić K, Legat A (2012) An electrochemical impedance study of the corrosion protection of artificially formed patinas on recent bronze. Electrochim Acta 83:28-39

[6] Muresan L, Varvara S, Stupnišek-Lisac E, Otmačić H, Marušić K, Horvat-Kurbegović S, Robbiola L, Rahmouni K, Takenouti H (2007) Protection of bronze covered with patina by innoxious organic substances. Electrochim Acta 52:7770-7779

[7] Marušić K, Otmačić-Ćurković H, Takenouti H (2011) Inhibiting effect of 4-methyl-1-p-tolylimidazole to the corrosion of bronze patinated in sulphate medium. Electrochim Acta 56:7491-7502

[8] Robbiola L, Blengino JM, Fiaud C (1998) Morphology and mechanisms of formation of natural patinas on archaeological Cu–Sn alloys. Corros Sci 40:2083-2111

[9] Cano E, Lafuente D (2013) Corrosion inhibitors for the preservation of metallic heritage artefacts. In: Dillmann P, Watkinson D, Angelini E, Adriaens A (eds) European Federation of Corrosion (EFC) Series, Corrosion and Conservation of Cultural Heritage Metallic Artefacts. Woodhead Publishing, Cambridge

[10] Walker R (2000) Aqueous Corrosion of Tin-Bronze and Inhibition by Benzotriazole. Corrosion 56:1211-1219

[11] Taylor RJ, MacLeod ID (1985) Corrosion of Bronzes on Shipwrecks. Corrosion 41:100-104

[12] Balbo A, Chiavari C, Martini C, Monticelli C (2012) Effectiveness of corrosion inhibitor films for the conservation of bronzes and gilded bronzes. Corros Sci 59:204-212

[13] Dermaj A, Hajjaji N, Joiret S, Rahmouni K, Srhiri A, Takenouti H, Vivier V (2007) Electrochemical and spectroscopic evidences of corrosion inhibition of bronze by a triazole derivative. Electrochim Acta 52:4654-4662

[14] Allam NK, Nazeer AA, Ashour EA (2009) A review of the effects of benzotriazole on the corrosion of copper and copper alloys in clean and polluted environments. J Appl Electrochem 39:961-969

[15] Rotarua I, Varvara S, Gaina L, Muresan LM (2014) Antibacterial drugs as corrosion inhibitors for bronze surfaces in acidic solutions. Appl Surf Sci 321:188-196

[16] Qafsaoui W, Kendig M, Perrot H, Takenouti H (2013) Coupling of electrochemical techniques to study copper corrosion inhibition in 0.5 mol.L^{-1}NaCl by 1-pyrrolidine dithiocarbamate. Electrochim Acta 87:348-360

[17] Qafsaoui W, Kendig MW, Perrot H, Takenouti H (2015) Effect of 1-pyrrolidine dithiocarbamate on the galvanic coupling resistance of intermetallics – Aluminum matrix during corrosion of AA 2024-T3 in a dilute NaCl. Corros Sci 92:245-255

[18] Qafsaoui W, Et Taouil A, Kendig M, Cachet H, Joiret S, Perrot H, Takenouti H (2018) Coupling of electrochemical, electrogravimetric and surface analysis techniques to study dithiocarbamate / bronze interactions in chloride media. Corros Sci 130:190-202

[19] Qin TT, Li J, Luo HQ, Li M, Li NB (2011) Corrosion inhibition of copper by 2,5 dimercapto-1,3,4-thiadiazole monolayer in acidic solution. Corros Sci 53:1072-1078

[20] Yadav M, Sharma D (2010) Inhibition of corrosion of copper by 2,5-dimercapto-1,3,4-thiadiazole in 3.5% NaCl solution. Indian J Chem Techn 17:95-101

[21] Kendig M, Hon M (2005) A Hydrotalcite-Like Pigment Containing an Organic Anion Corrosion Inhibitor. Electrochem Solid St 8:B10-B11

[22] Kendig M, Hon M, Sinko J (2006) Inhibition of Oxygen Reduction on Copper in Neutral Sodium Chloride Corrosion Inhibition - Non Ferrous Metals. ECS Transactions 1:119-129

[23] Kendig M, Hon M (2004) Environmentally Triggered Release of Oxygen-Reduction Inhibitors from Inherently Conducting Polymers. Corrosion 60:1024-1030

[24] Kendig M, Yan C (2004) Critical Concentrations for Selected Oxygen Reduction Reaction Inhibitors. J Electrochem Soc 151:B679-B682

[25] Kendig M, Kinlen P (2007) Demonstration of Galvanically Stimulated Release of a Corrosion Inhibitor: Basis for "Smart" Corrosion Inhibiting Materials Corrosion, Passivation, and Anodic Films. J Electrochem Soc154:C195-C201

[26] Bernard MC, Joiret S (2009) Understanding corrosion of ancient metals for the conservation of cultural heritage. Electrochim Acta 54:5199-5205

[27] Joy VT, Srinivasan TKK (2001) Ft-SERS studies on 1,3-thiazolidine-2-thione, 2,5-dimercapto-1,3,4-thiadiazole and 2-thiouracil adsorbed on chemically deposited silver films. J Raman Spectrosc 32:785–793

[28] Pope JM, Sato T, Shoji E, Buttry DA, Sotomura T, Oyama N (1997) Spectroscopic identification of 2,5-dimercapto-1,3,4-thiadiazole and its lithium salt and dimer forms. J Power Sources 68:739-742

[29] Maiti N, Chadha R, Das A, Kapoor S (2016) Surface Selective Bending of 2,5-Dimercapto-1,3,4-thiadiazole (DMTD) on Silver and Gold nanoparticles: A Raman and DFT study. Roy Soc Chem Adv 6:62529-62539

[30] Edwards HGM, Johnson AF, Lawson EE (1995) Structural determination of substituted mercaptothiadiazoles using FT-Raman and FT-IR spectroscopy. J Mol Struct 351:51-63

[31] Matsumoto F, Ozaki M, Inatomi Y, Paulson SC, Oyama N (1999) Studies on the Adsorption Behavior of 2,5-Dimercapto-1,3,4-thiadiazole and 2-Mercapto-5-methyl-1,3,4-thiadiazole at Gold and Copper Electrode Surfaces. Langmuir 15:857-865

[32] Huang L, Shen J, Ren J, Meng Q, Yu T (2001) The adsorption of 2,5-Dimercapto-1,3,4-thiadiazole (DMTD) on copper surface and its binding behavior. Chinese Sci Bull 46:1-4

[33] Huang L, Tang F, Hu B, Shen J, Yu T, Meng Q (2001) Chemical Reactions of 2,5-Dimercapto-1,3,4-thiadiazole (DMTD) with Metallic Copper, Silver and Mercury. J Phys Chem B 105:7984-7989

[34] Finšgar M (2013) 2-Mercaptobenzimidazole as a copper corrosion inhibitor: Part II. Surface analysis using X-ray photoelectron spectroscopy. Corros Sci 72:90-98

[35] Finšgar M, Kovač J, Milošev I (2010) Surface analysis of 1-hydroxybenzotriazole and benzoltriazole adsorbed on Cu by X-ray photoelectron spectroscopy. J Electrochem Soc 157:C52-C60

[36] Finšgar M (2013) EQCM and XPS analysis of 1,2,4-triazole and 3-amino-1,2,4-triazole as copper corrosion inhibitors in chloride solution. Corros Sci 77:350-359

[37] Finšgar M (2013) 2-Mercaptobenzimidazole as a copper corrosion inhibitor: Part I. Long-term immersion, 3D-profilometry, and electrochemistry. Corros Sci 72:82-89

[38] Finšgar M, Kek Merl D (2014) 2-Mercaptobenzoxazole as a copper corrosion inhibitor in chloride solution: electrochemistry, 3D-profilometry, and XPS surface analysis. Corros Sci 80:82-95

[39] Laibinis PE, Whitesides GM, Allara DL, Tao YT, Parikh AN, Nuzzo RG (1991) Comparison of the structures and wetting properties of self-assembled monolayers on n-alkanethiols on the coinage metal surfaces, copper, silver and gold. J Am Chem Soc 113:7152-7167

[40] Qafsaoui W, Kendig MW, Joiret S, Perrot H, Takenouti H (2016) Ammonium pyrrolidine dithiocarbamate adsorption on copper surface in neutral chloride media. Corros Sci 106:96-107

[41] Naumkin AV, Kraut-Vass A, Gaarenstroom SW, Powell CJ (2003) NIST Standard Reference Database 20, Version 4.1, <http://srdata.nist.gov/xps/>

[42] Muilenberg GE (ed) (1979) Handbook of X-ray Photoelectron Spectroscopy. Perkin-Elmer Corporation, Eden Prairie, Minnesota

[43] Milošev I, Strehblow HH (2003) Electrochemical behaviour of Cu-xZn alloys in borate buffer solution at pH 9.2. J Electrochem Soc 150:B517-B524

[44] Squarcialupi MC, Bernardini GP, Faso V, Atrei A, Rovida G (2002) Characterisation by XPS of the corrosion patina formed on bronze surfaces. J Cult Herit 3:199–204

[45] Galtayries A, Bonnelle JP (1995) XPS and ISS Studies on the Interaction of H_2S with Polycrystalline Cu, Cu_2O and CuO Surfaces. Surf Interface Anal 23:171-179

[46] Chawla SK, Sankarraman N, Payer JH (1992) Diagnostic spectra for XPS analysis of Cu-O-S-H compounds. J Electron Spectrosc 61:1-18

[47] Zucchi F, Frignani A, Grassi V, Trabanelli G, DalColle M (2007) The formation of a protective layer of 3-mercapto-propyl-trimethoxy-silane on copper. Corros Sci 49:1570-1583

[48] Deslouis C, Tribollet B, Mengoli G, Musiani MM (1988) Electrochemical behavior of copper in neutral aerated chloride solution. I. Steady-state investigation. J Appl Electrochem 18:374-383

[49] Lee HP, Nobe K (1986) Kinetics and mechanisms of Cu electrodissolution in chloride media. J Electrochem Soc 133:2035-2043

[50] Kear G, Barker BD, Walsh FC (2004) Electrochemical corrosion of unalloyed copper in chloride media-a critical review. Corros Sci 46:109-135

[51] Shaban A, Kálmán E, Telegdi J (1998) An investigation of copper corrosion inhibition in chloride solutions by benzo-hydroxamic acids. Electrochim Acta 43:159-163

[52] Souissi N, Sidot E, Bousselmi L, Triki E, Robbiola L (2007) Corrosion behaviour of Cu–10Sn bronze in aerated NaCl aqueous media – Electrochemical investigation. Corros Sci 49:3333-3347

[53] Qafsaoui W, Kendig MW, Perrot H, Takenouti H (2008) Corrosion Inhibition of Copper by Selected Thiol Compounds. ECS Transactions 13:123-132

[54] Huang L, Tang F, Hu B, Shen J, Yu T, Meng Q (2001) Chemical Reactions of 2,5 Dimercapto-1,3,4-thiadiazole (DMTD) with Metallic Copper, Silver, and Mercury. J Phys Chem B 105:7984-7989

[55] Shouji E, Yokoyama Y, Pope JM, Oyama N, Buttry DA (1997) Electrochemical and Spectroscopic Investigation of the Influence of Acid-Base Chemistry on the Redox Properties of 2,5-Dimercapto-1,3,4-thiadiazole. J Phys Chem B 101:2861-2866

[56] Picart S, Geniès E (1996) Electrochemical study of 2,5-dimercapto-1,3,4-thiadiazole in acetonitrile. J Electroanal Chem 408:53-60

[57] Tatsuma T, Yokoyama Y, Buttry DA, Oyama N (1997) Electrochemical Polymerization and Depolymerization of 2,5-Dimercapto-1,3,4-thiadiazole, QCM and Spectroscopic Analysis. J Phys Chem B 101:7556-7562

[58] Barsoukov E, Macdonald JR (2005) Impedance spectroscopy, Theory, Experiment, and Applications. John Wiley and Sons, New York

[59] Cole KS, Cole RH (1941) Dispersion and absorption in dielectrics- I Alternating current characteristics. J Chem Phys 9:341-351

[60] Epelboin I, Gabrielli C, Keddam M, Takenouti H (1981) A-C impedance measurements applied to corrosion studies and corrosion rate determination. In: Mansfeld F, Bertocci U (eds) Electrochemical Corrosion Testing STP 727. American Society for Testing and Materials, Philadelphia

[61] Benoit M, Bataillon C, Gwinner B, Miserque F, Orazem ME, Sánchez-Sánchez CM, Tribollet B, Vivier V (2016) Comparison of different methods for measuring the passive film thickness on metals. Electrochim Acta 201:340-347

Table captions

Table 1: Composition of the industrial bronze.

Table 2: EDX analysis of bronze surface after 24 hours immersion in 30 g L^{-1} NaCl without and with DMTD.

Table 3: Vibrational wavenumbers and assignments for DMTD molecule, A species, B species, monothiolate and dithiolate.

Figure captions

Fig. 1: SEM images of bronze surface after 24 h immersion time in 30 g L^{-1} NaCl with 0.1 mM (a), 1 mM (b) and 10 mM DMTD (c).

Fig. 2: Raman spectra collected on DMTD molecule, Cu^{II}-DMTD complex and on bronze electrode after 24 h immersion in 30 g L^{-1} NaCl without or with 0.1 mM or 10 mM DMTD.

Fig. 3: Raman spectra collected on bronze and copper electrodes after 24 h immersion in 30 g L^{-1} NaCl with 1 mM or 10 mM DMTD.

Fig. 4: Schematic representation of monodentate (a) and bidentate (b) adsorption of DMTD on bronze surface respectively at 10 mM and 1 mM in 30 g L^{-1} NaCl.

Fig. 5: Survey XPS spectra of bronze electrode after 24 h immersion in 30 g L^{-1} NaCl without or with 10 mM DMTD.

Fig. 6: Cu2p and CuLMM spectra of bronze electrode after 24 h immersion in 30 g L^{-1} NaCl without or with 10 mM DMTD. Dashed lines indicate shake-up satellites of Cu2p.

Fig. 7: Open circuit potential plots (a) for bronze during one hour exposure time in 30 g L^{-1} NaCl without or with different concentrations of DMTD and polarization plots (b) after exposure; stationary electrode at 20 °C.

Fig. 8: Effect of 10 mM DMTD on the electrode kinetics of Cu, Sn, Pb and Zn electrodes in 30 g L^{-1} NaCl after one hour of immersion; stationary electrodes at 20 °C.

Fig. 9: Nyquist diagrams of bronze after 24 hours exposure time in 30 g L^{-1} NaCl + DMTD at different concentrations; stationary electrode at 20 °C.

Symbols = experimental data; and crosses = calculated data.

Fig. 10: Electrical equivalent circuit to reproduce experimental impedance spectra for bronze electrode in NaCl solution without or with DMTD.

Fig. 11: R_f (a), C_f (b), R_t (c) and C_d (d) change as a function of immersion time for bronze / 30 g L^{-1} NaCl + DMTD at different concentrations; stationary electrode at 20 °C.

Fig. 12: R_F (a) and R_p (b) change as a function of immersion time in bronze / 30 g L^{-1} NaCl + DMTD at different concentrations; stationary electrode at 20 °C.

Fig. 13: Thickness of films formed on bronze, determined from C_∞ (full circles) and C_f (open circles), as a function of immersion time in 30 g L^{-1} NaCl + DMTD at different concentrations; stationary electrode at 20 °C.

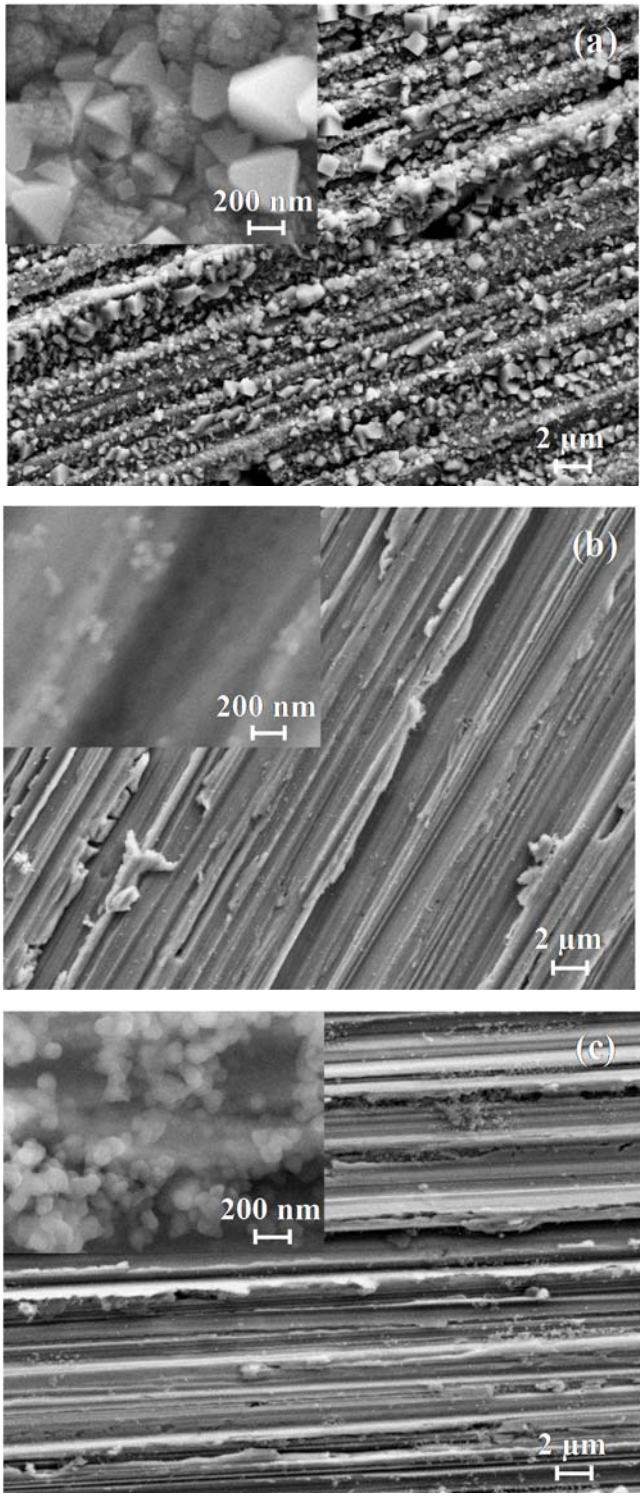

Figure 1: SEM images of bronze surface after 24 h immersion time in 30 g L^{-1} NaCl with 0.1 mM (a), 1 mM (b) and 10 mM DMTD (c).

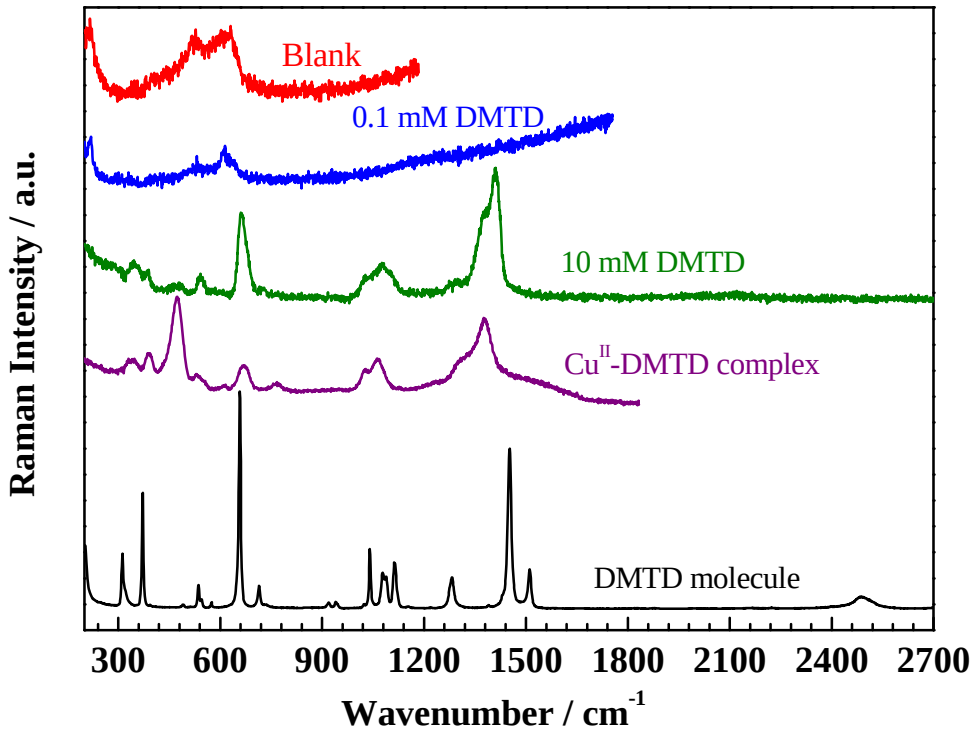

Figure 2: Raman spectra collected on DMTD molecule, Cu^{II}-DMTD complex and on bronze electrode after 24 h immersion in 30 g L^{-1} NaCl without or with 0.1 mM or 10 mM DMTD.

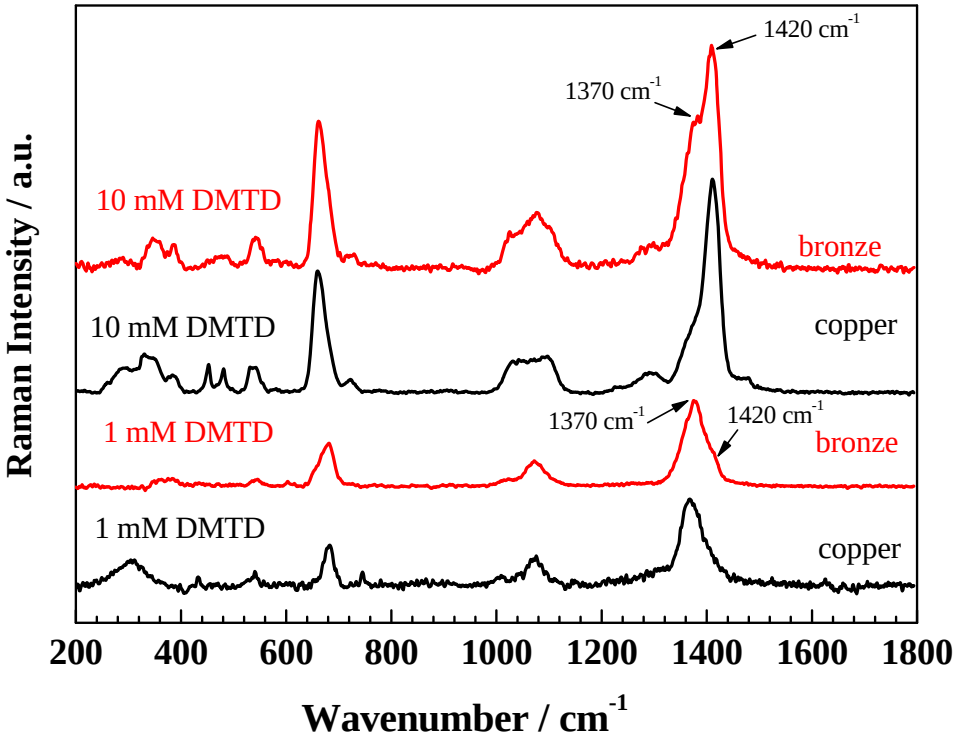

Figure 3: Raman spectra collected on bronze and copper electrodes after 24 h immersion in 30 g L^{-1} NaCl with 1 mM or 10 mM DMTD.

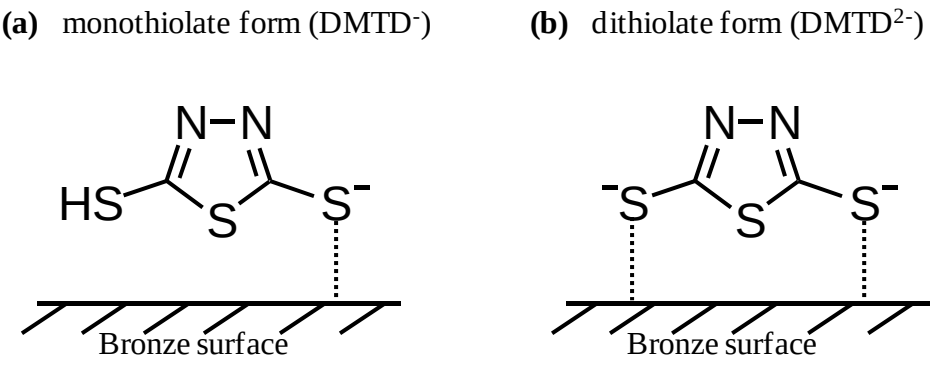

Figure 4: Schematic representation of monodentate (a) and bidentate (b) adsorption of DMTD on bronze surface respectively at 10 mM and 1 mM in 30 g L^{-1} NaCl.

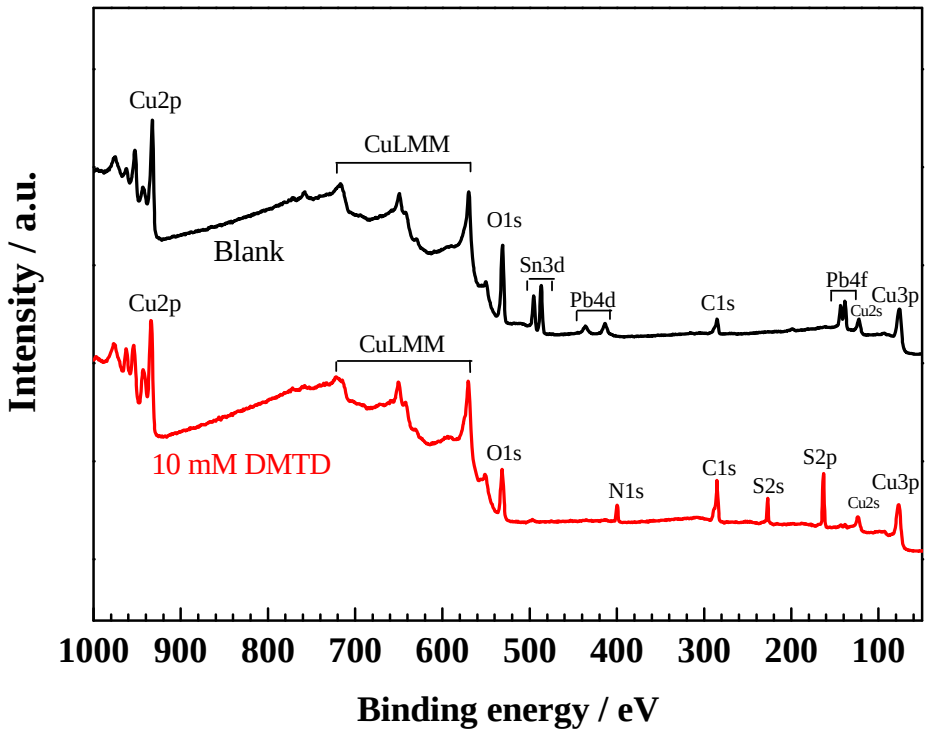

Figure 5: Survey XPS spectra of bronze electrode after 24 h immersion in 30 g L^{-1} NaCl without or with 10 mM DMTD.

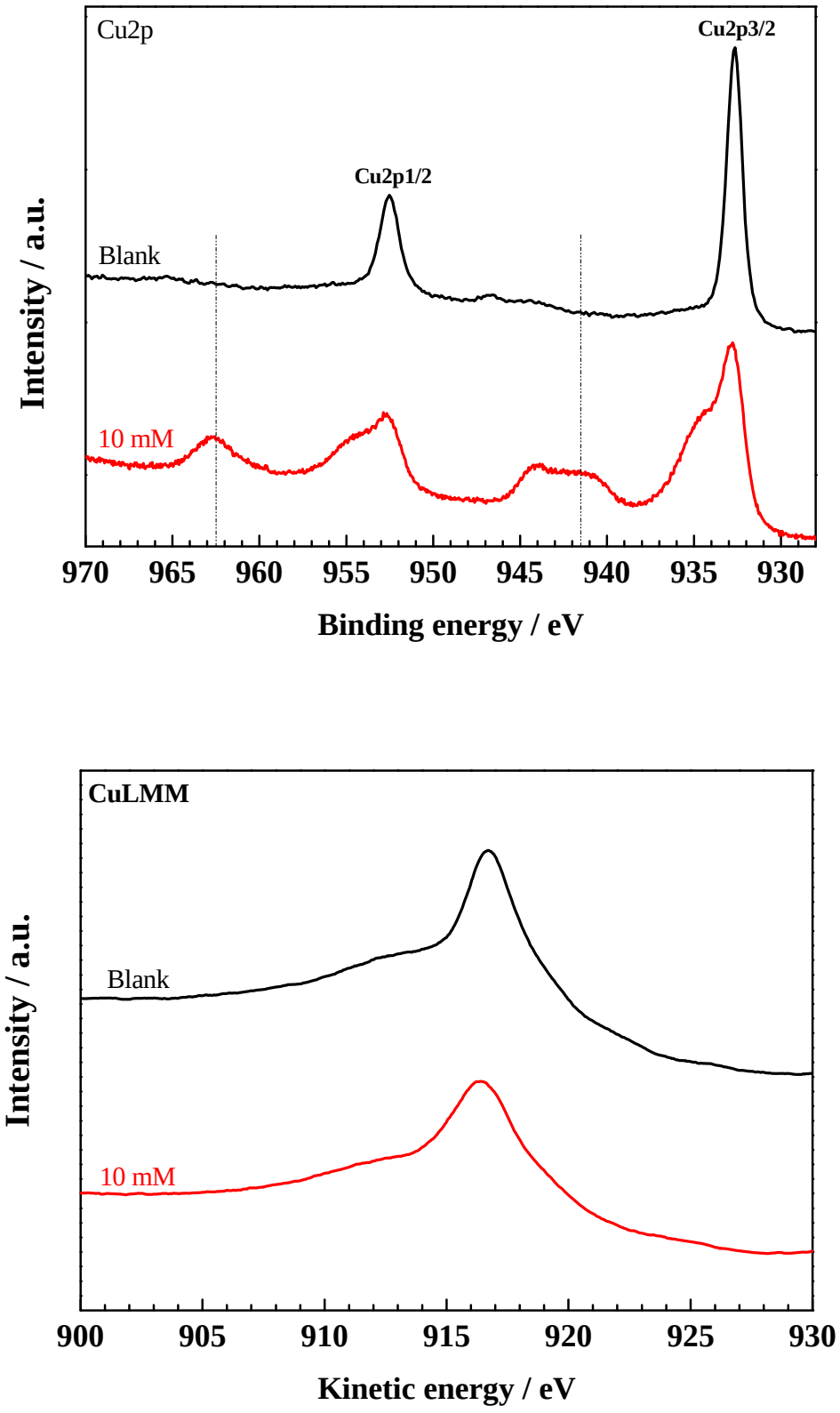

Figure 6: Cu2p and CuLMM spectra of bronze electrode after 24 h immersion in 30 g L^{-1} NaCl without or with 10 mM DMTD. Dashed lines indicate shake-up satellites of Cu2p.

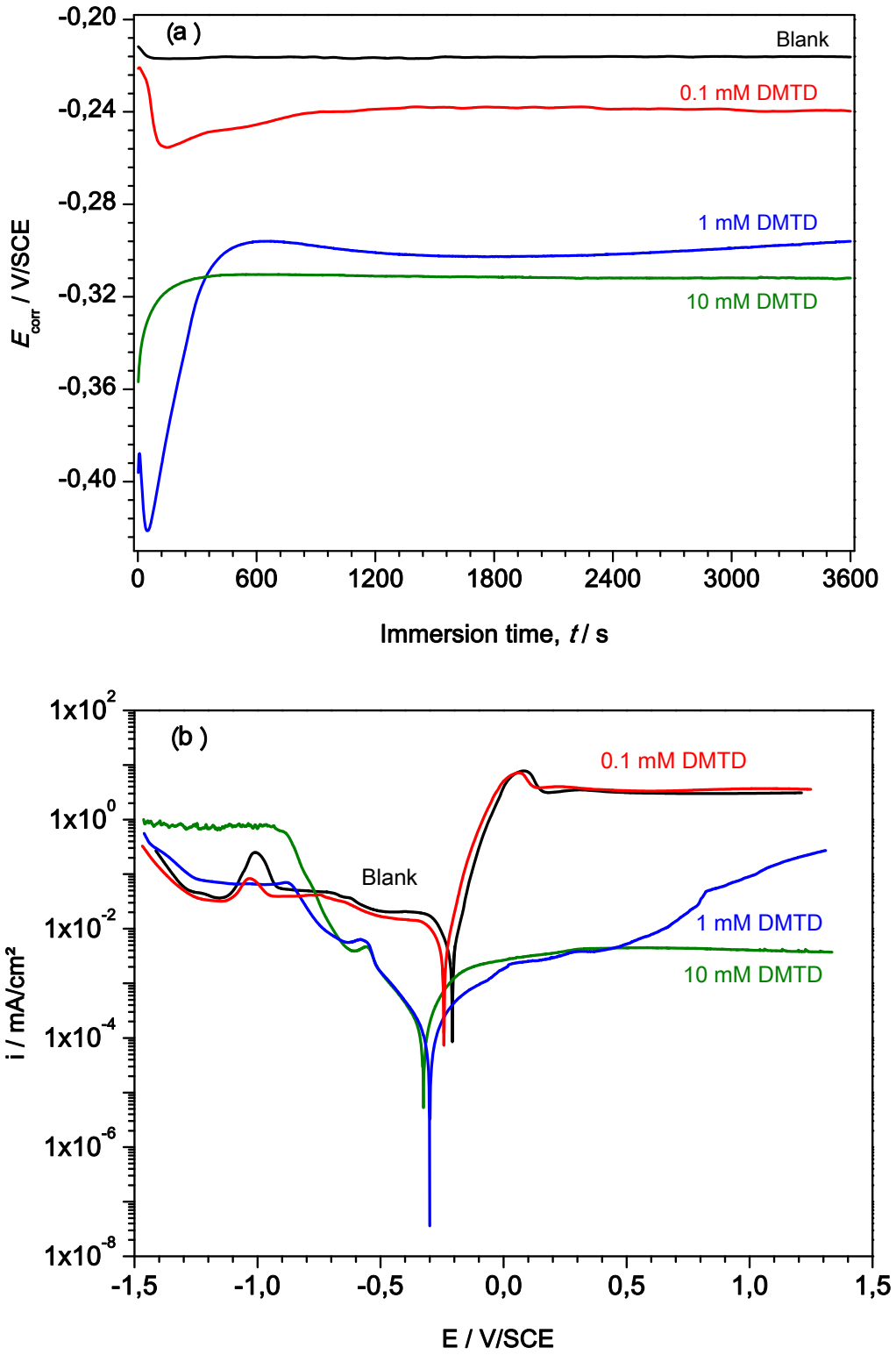

Figure 7: Open circuit potential plots (a) for bronze during one hour exposure time in 30 g L^{-1} NaCl without or with different concentrations of DMTD and polarization plots (b) after exposure; stationary electrode at 20 °C.

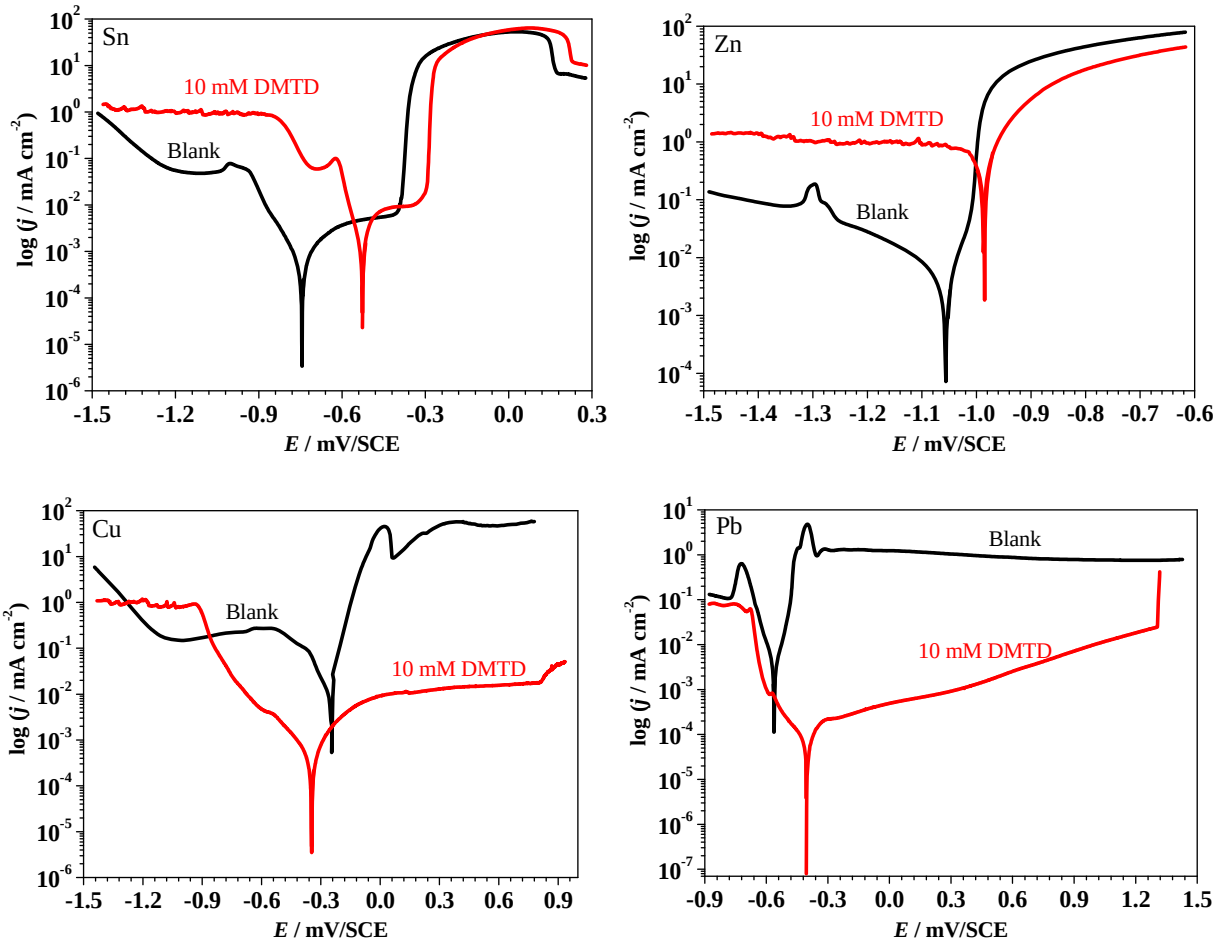

Figure 8: Effect of 10 mM DMTD on the electrode kinetics of Cu, Sn, Pb and Zn electrodes in 30 g L^{-1} NaCl after one hour of immersion; stationary electrodes at 20 °C.

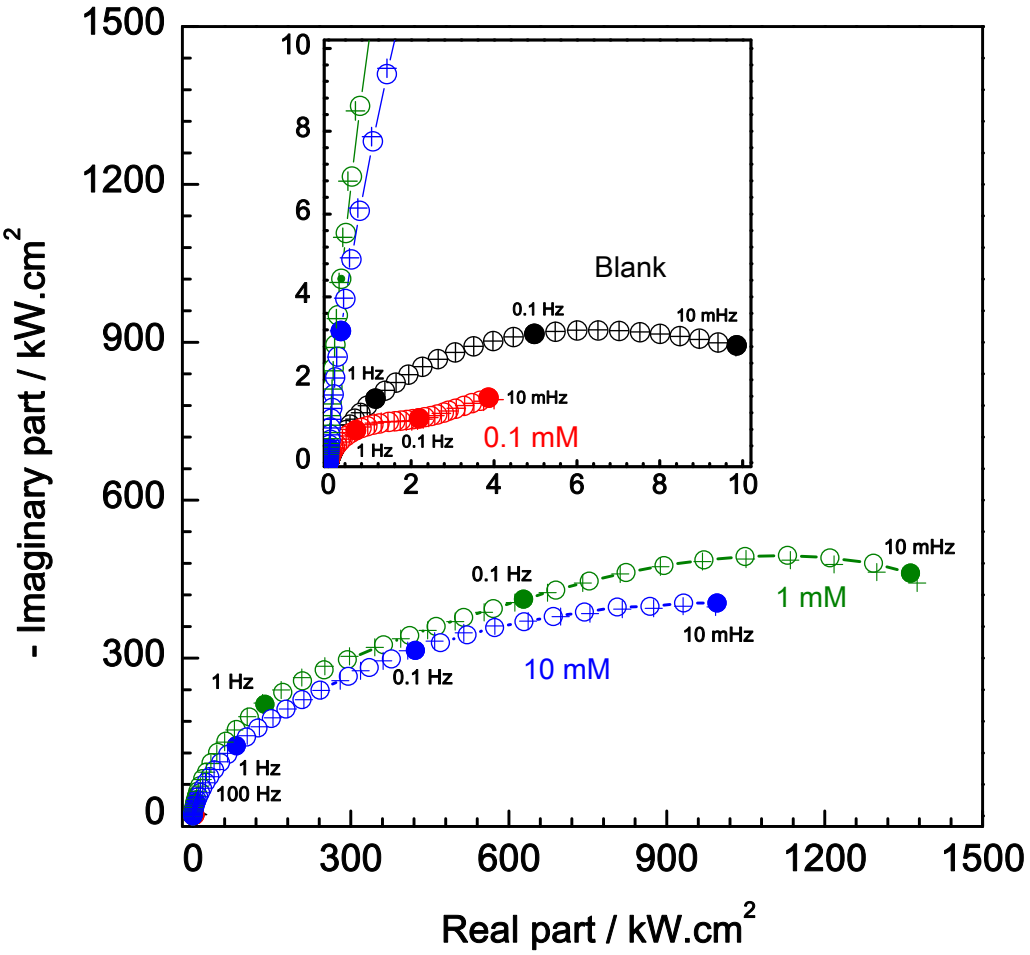

Figure 9: Nyquist diagrams of bronze after 24 hours exposure time in 30 g L^{-1} NaCl + DMTD at different concentrations; stationary electrode at 20 °C.

Symbols = experimental data; and crosses = calculated data.

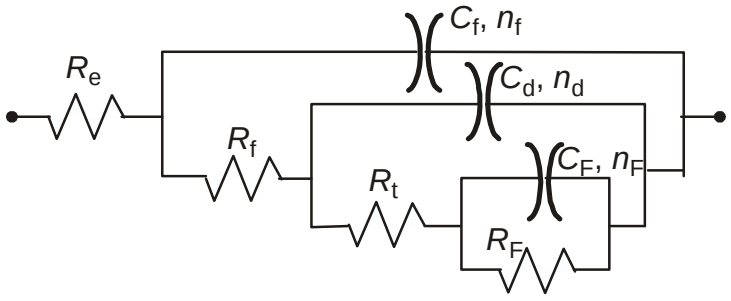

Figure 10: Electrical equivalent circuit to reproduce experimental impedance spectra for bronze electrode in NaCl solution without or with DMTD.

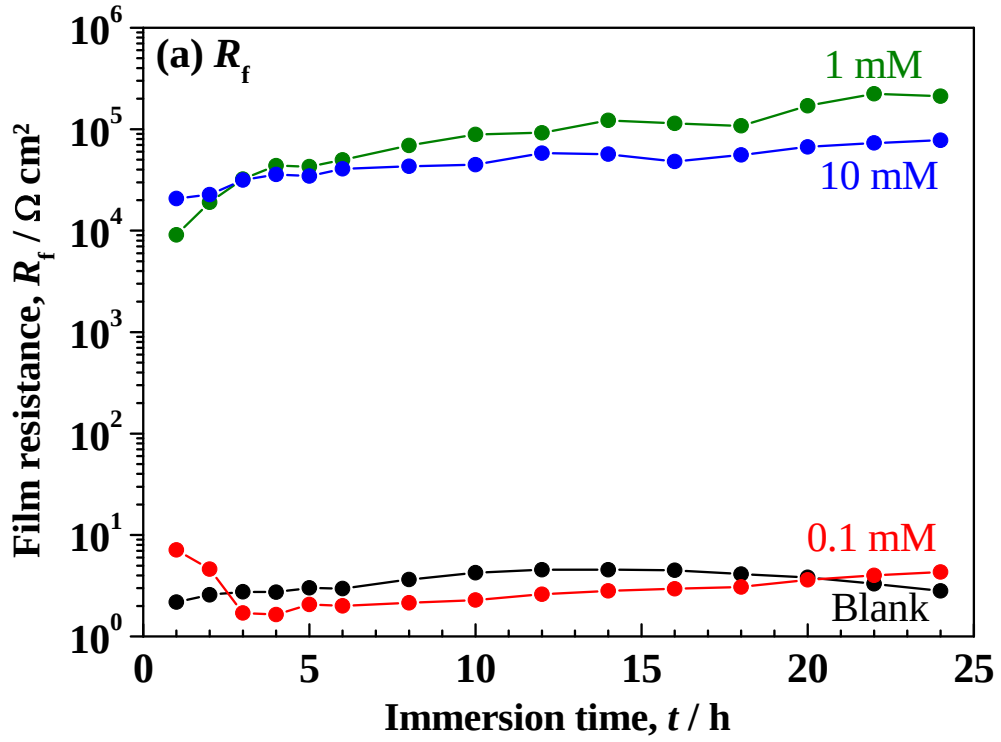
(a) R_f
1 mM
10 mM
0.1 mM
Blank
Film resistance, R_f / Ω cm²
Immersion time, t / h

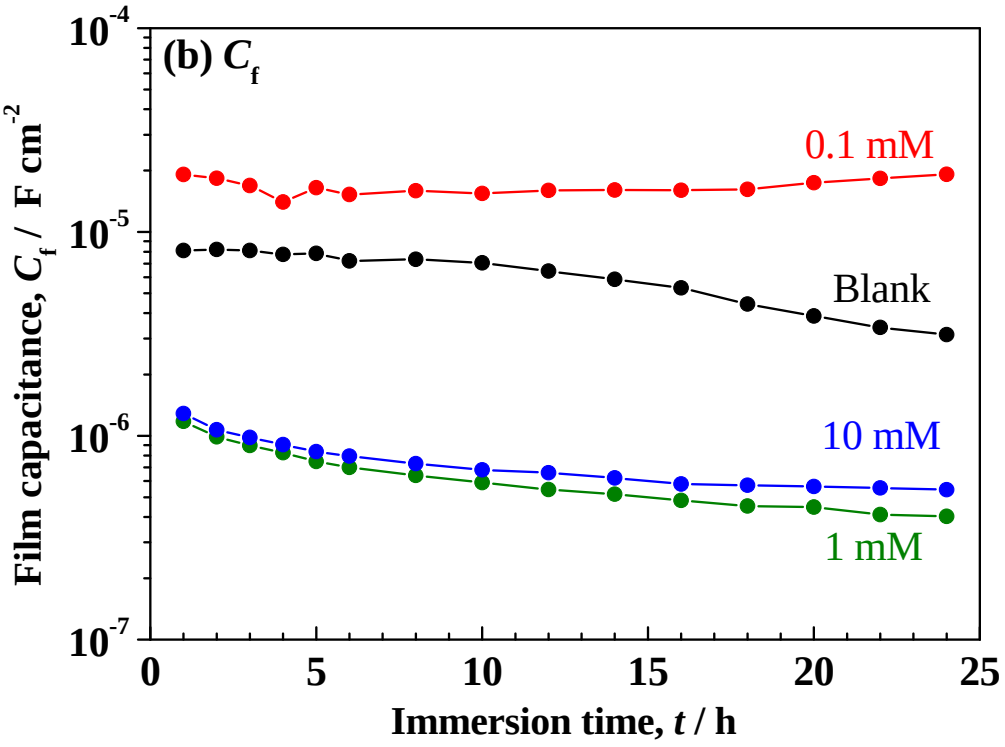
(b) C_f
0.1 mM
Blank
10 mM
1 mM
Film capacitance, C_f / F cm^{-2}
Immersion time, t / h

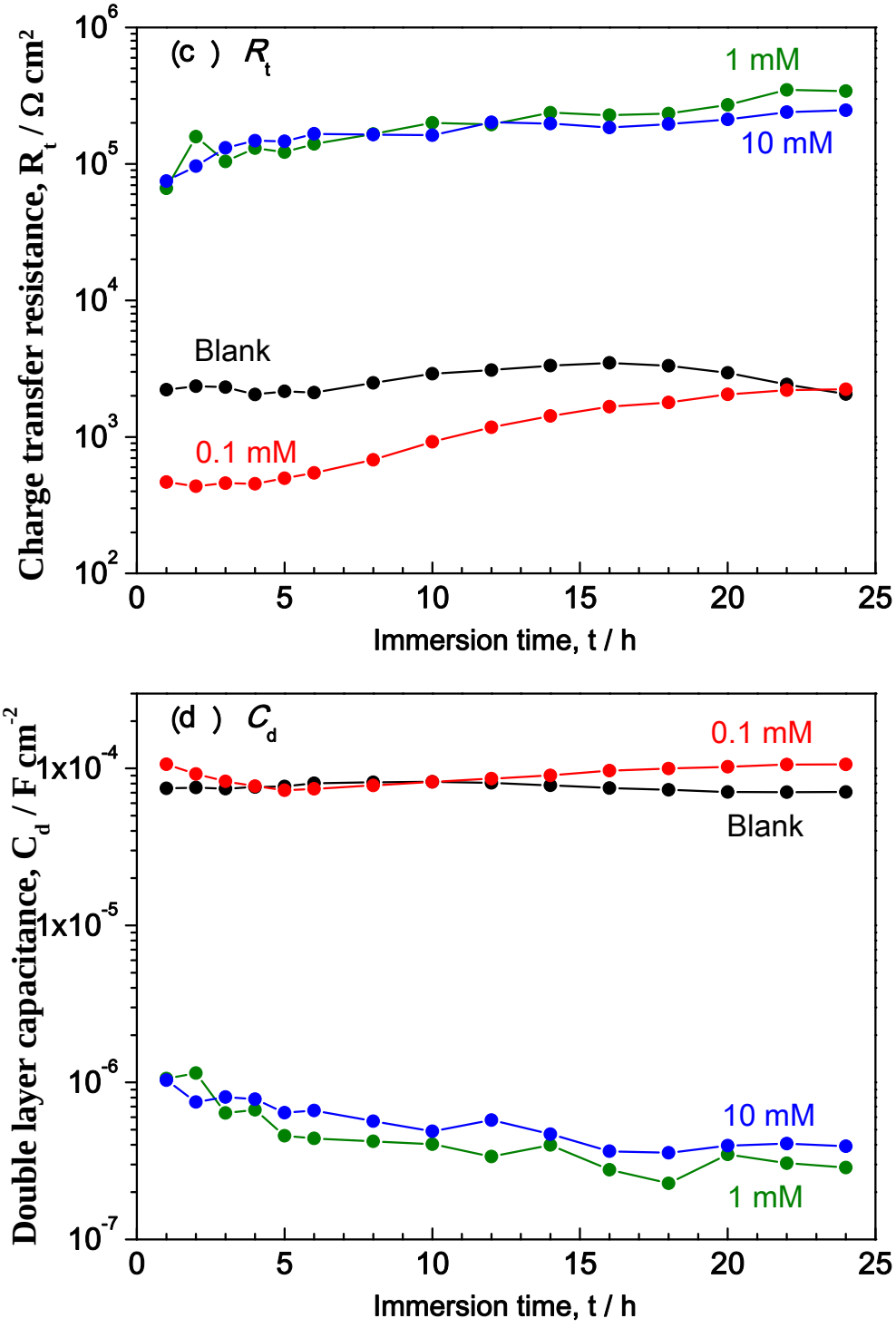

Figure 11: R_f (a), C_f (b), R_t (c) and C_d (d) change as a function of immersion time for bronze / 30 g L^{-1} NaCl + DMTD at different concentrations; stationary electrode at 20 °C.

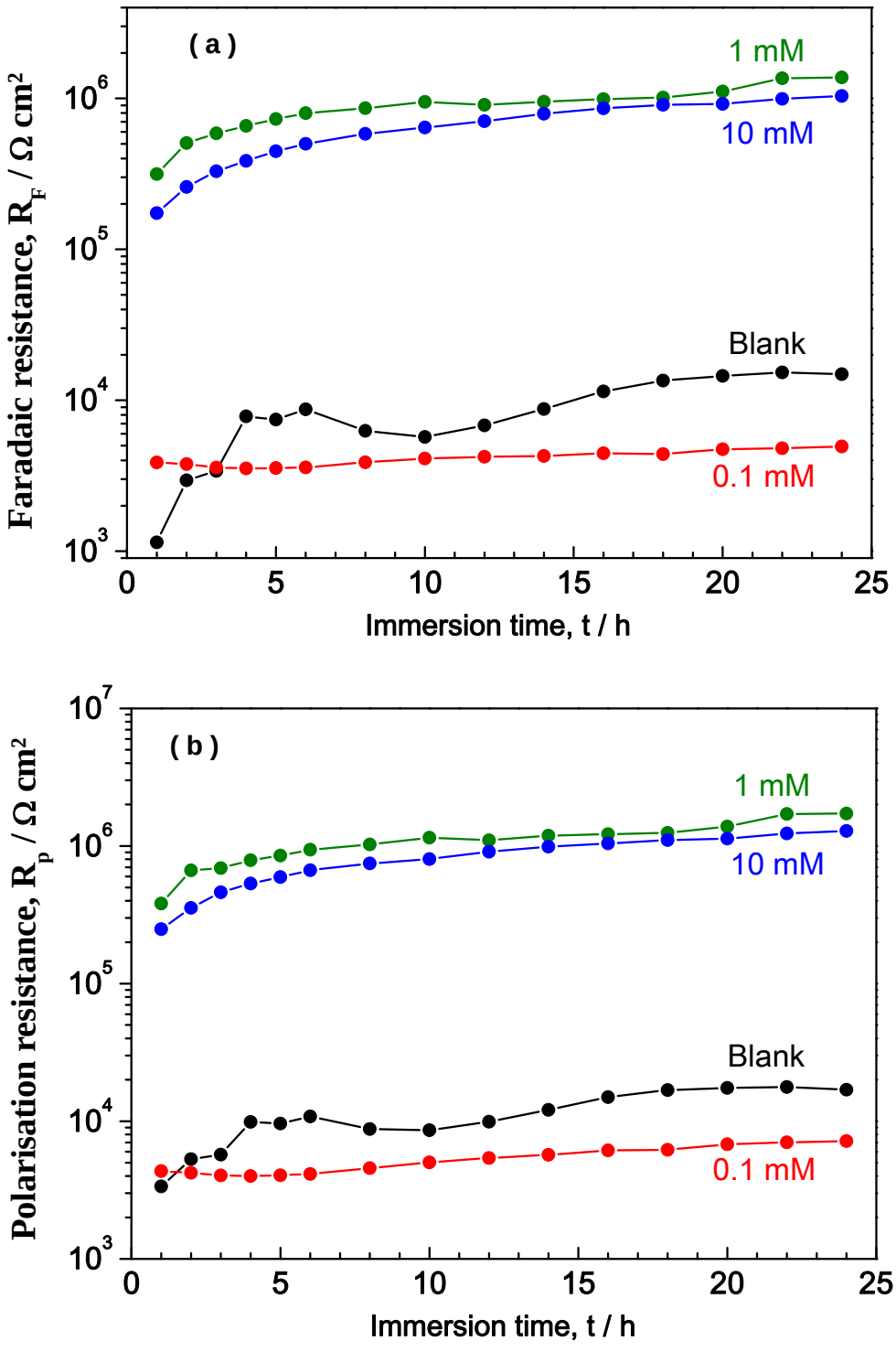

Figure 12: R_F (a) and R_p (b) change as a function of immersion time in bronze / 30 g L^{-1} NaCl + DMTD at different concentrations; stationary electrode at 20 °C.

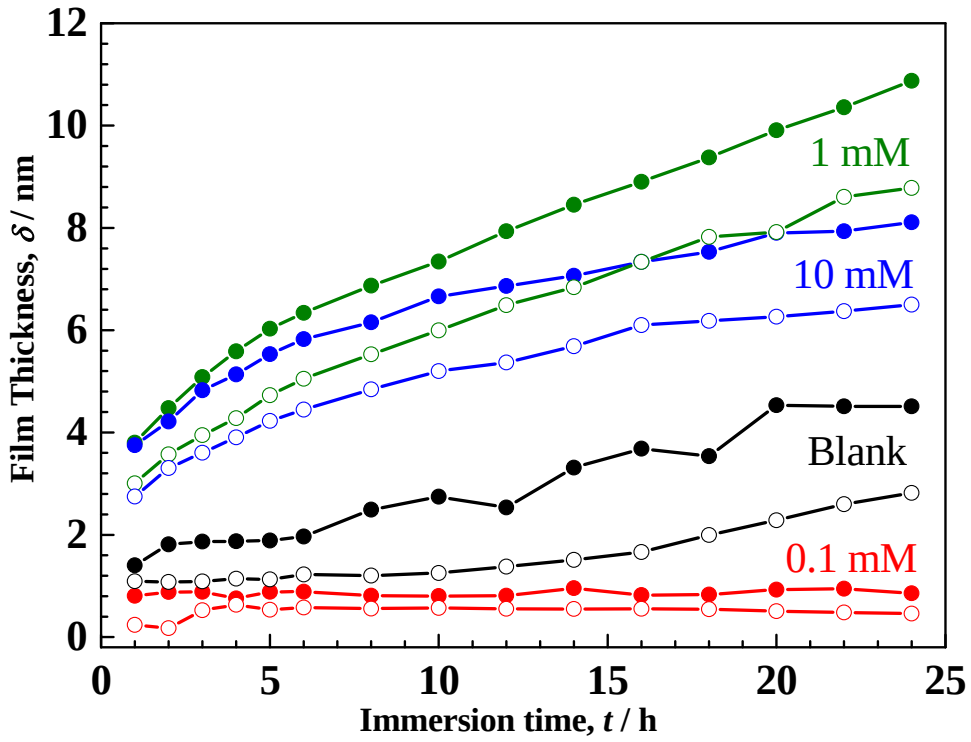

Figure 13: Thickness of films formed on bronze, determined from C_{∞} (full circles) and C_f (open circles), as a function of immersion time in 30 g L^{-1} NaCl + DMTD at different concentrations; stationary electrode at 20 °C.

Graphical Abstract

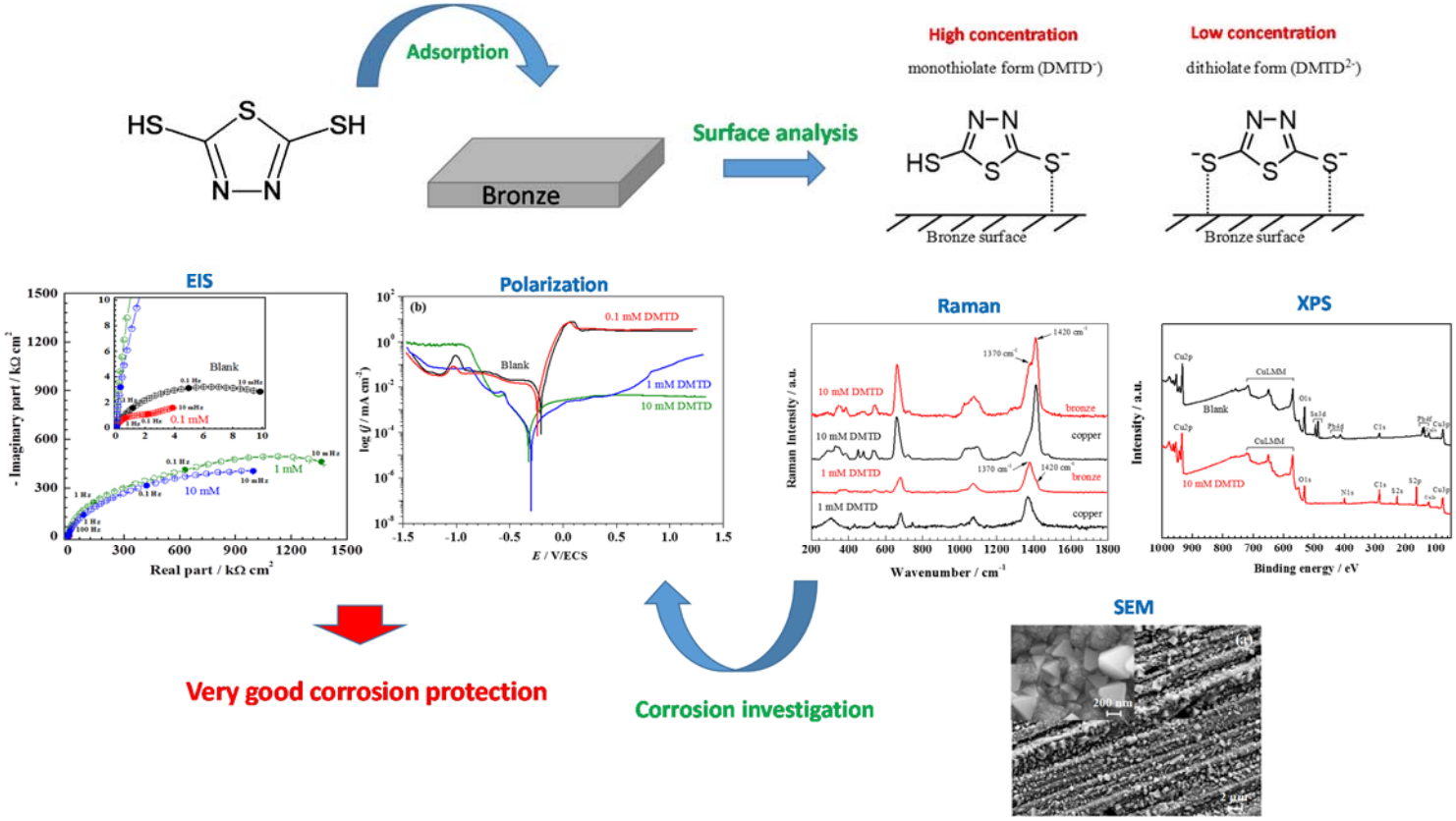

Table 1: Composition of the industrial bronze.

	Cu	Sn	Zn	Pb	P	Ni	Fe	Al	Mn
at %	91.050	6.227	1.570	0.482	0.282	0.280	0.104	0.0123	0.00011

Table 2: EDX analysis of bronze surface after 24 hours immersion in 30 g L^{-1} NaCl without and with DMTD.

Element at %	30 g L^{-1} NaCl	30 g L^{-1} NaCl + 0.1 mM DMTD	30 g L^{-1} NaCl + 1 mM DMTD	30 g L^{-1} NaCl + 10 mM DMTD
Cu	76.8	70.1	91.8	89.4
Sn	6.30	10.2	3.3	6.5
O	16.9	19.7	0.70	0.81
S	-	-	4.20	3.29

Table 3: Vibrational wavenumbers and assignments for DMTD molecule, A species, B species, monothiolate and dithiolate.

		Raman wavenumber (cm^{-1})			
DMTD molecule	A species (1 mM)	B species (10 mM)	Monothiolate ($DMTD^{-}$) [28]	Dithiolate ($DMTD^{2-}$) [27,28]	Assignment [27-30]
2490					S-H str.
1515		1477	1500		C=N str. asym
1455	1365	1410	1405	1375	C=N str. sym
1110		1100			CNNC def. ip
1070	1070	1070		1070	ring def.
1040		1035	1025	1025	N-N str.
715		715	722		C-S-C str. asym
650	680	660	665	670	C-S-C str. sym

str: stretching ; sym: symetric ; asym: antisymetric ; def: deformation ; ip: in plane